

# Neutron Captures in Borated Polyethylene: An Analysis of the Quenching Measurement Data from MicroCHANDLER at TUNL

By Jacob Steenis<sup>1</sup>, Connor Awe<sup>2</sup>, Shengchao Li<sup>3</sup>, and J. M. Link<sup>3</sup>

<sup>1</sup>Grinnell College

<sup>2</sup>Triangle Universities Nuclear Laboratory

<sup>3</sup>Center for Neutrino Physics, Virginia Tech

## ABSTRACT

This summer, the MicroCHANDLER particle detector was brought to the tandem accelerator at Triangle Universities Nuclear Laboratory to measure the detector's quenching factor using a beam of neutrons. Specifically, the goal was to obtain preliminary data to understand how MicroCHANDLER responds to protons that recoil off of fast neutrons. To prevent thermal neutrons from interfering with data acquisition while the beam was on, MicroCHANDLER was housed in a structure of borated polyethylene. Although this structure significantly attenuates thermal neutrons in the target room, neutron captures on hydrogen within the borated polyethylene often generate 2.2MeV gammas that can be seen in MicroCHANDLER. In fact, these neutron captures appear in the delta time plots with an exponential growth structure. Examining this growth structure reveals that setting the event window towards the beginning of the beam period will allow us to minimize the number of neutron capture gammas that register in the detector. Additionally, having identified this 2.2MeV gamma feature provides another calibration point for future runs. Overall, this study acts as a first step in determining how the turn-on of neutron captures in borated polyethylene appears in our data. More data is required to be able to see a turnover in the rate of neutron captures as the majority of neutrons have already captured in the borated polyethylene. New data would also allow us to see the exponential decay in capture rates that should immediately follow turnover.

*Keywords: boron 10, hydrogen, thermal neutron capture, borated polyethylene, CHANDLER.*

## 1. Introduction

In June, the MicroCHANDLER (Carbon Hydrogen Anti-Neutrino Detector with a Lithium Enhanced Raghavan optical lattice) particle detector was brought to the tandem accelerator at Triangle Universities Nuclear Laboratory (TUNL) to take data on proton quenching using a beam of fast neutrons. The detector was housed in a structure of borated polyethylene (BP) to attenuate thermal neutrons in the experimental hall. In general, BP serves as shielding against thermal neutrons due to the naturally high thermal neutron cross-section of boron 10. This property makes BP an obvious candidate to absorb thermal neutrons from the beam that bounce around in the hall.

However, while looking at ADC histograms from the first few test runs, we noticed an unexpected peak. In an attempt to determine the cause of this feature, we tried to determine whether it was beam-correlated. For these events, there are two types of beam correlation. The first type of beam-correlated events are those which are *directly* beam-correlated. These events are direct results of the beam production: beam neutrons and gammas

from the beamline. The second type of beam correlation stems from effects due to the beam simply being fired into the hall. For this study those events will primarily consist of neutron captures within the materials near the detector such as BP. In other words, this indirect beam correlation occurs when the beam is on, but it is not as closely related to the beam as the direct beam correlation. Therefore, when we use the phrase "beam-correlated" in this paper, it will refer to the indirect beam correlation pertaining to neutron captures.

After examining the data and specific events to ensure that the peak was truly beam-correlated, our initial hypothesis was that it was an artifact of neutron captures on boron 10 within the BP housing, thinking that this may correspond to a 4.4 MeV gamma. However, during the process of energy calibration and determining a better conversion between ADC count and energy in MeV, our hypothesis changed. Rather than claiming that this peak comes from neutron captures on boron 10, we now are confident that it instead corresponds to gamma rays generated by neutron captures on hydrogen. This process results in a

2.2MeV gamma which makes far more sense on MicroCHANDLER's ADC scale. This also makes intuitive sense given that hydrogen is naturally abundant in the hydrocarbons of the BP. Overall, the goal of this study is to provide an initial analysis of this data feature to show that the ADC peak seen in the data is truly a result of thermal neutron captures on hydrogen.

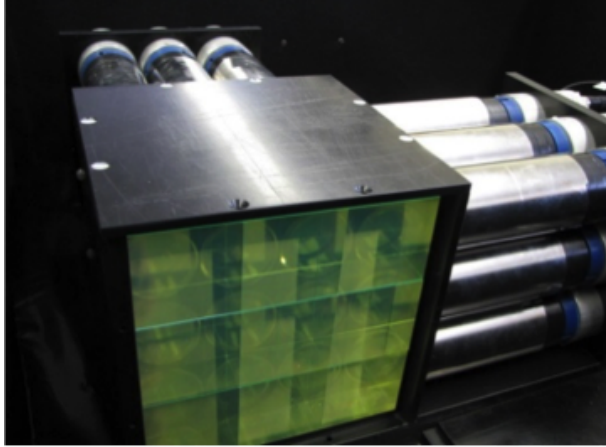


Figure 1a. An older version of MicroCHANDLER with one side of container removed.

## 2. Setup

### 2.1. MicroCHANDLER

MicroCHANDLER is a small-scale particle detector that utilizes wavelength-shifting plastic scintillator cubes to register charged particles that move through them. The detector is a 3x3x3 arrangement of these plastic cubes with neutron detection sheets separating the horizontal layers of cubes (see Figure 1a). This optical lattice structure of scintillator cubes was first developed by Raju Raghavan and is described in more detail in (C. Grieb, J. M. Link, and R.S. Raghavan). The neutron detection sheets contain a mixture of lithium-6 flouride micro-particles ( $\text{Li}^6\text{F}$ ) and micro-crystals of zinc sulfide scintillator that have been activated with silver ( $\text{ZnS:Ag}$ ). The scintillator cubes are green in order to absorb photons emitted by the neutron detection sheets and remit them so that they can be transmitted by total internal reflection to photomultiplier tubes (PMTs) attached to the detector. Pairing the detection sheets and plastic scintillators was first performed by SoLid (see Y. Abreu et al). Together, the cubes and neutron detection sheets are enclosed in a box with 3x3 arrangements of PMTs fixed to two adjacent sides of it (see Figure 1b). Note that each set of nine PMTs is assigned to a different coordinate axis. Channels 1 through 9 are assigned to the "X axis" while channels 10 through 18 are assigned to the "Y axis". MicroCHANDLER is essentially a smaller version of MiniCHANDLER which also utilizes the CHANDLER detector technology but is, instead, an 8x8x5 arrangement of scintillating cubes. A more detailed description of the CHANDLER technology and MiniCHANDLER itself can be found in (A. Haghghat et al, 2018).

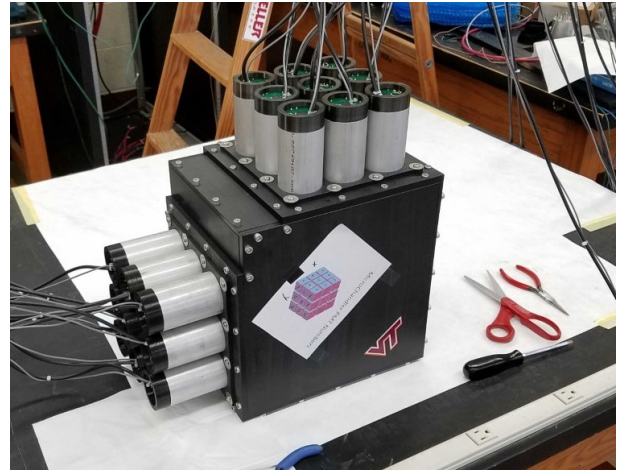


Figure 1b. MicroCHANDLER after having been newly rebuilt.

Image Credit: Connor Awe

The MicroCHANDLER particle detector was housed in two different concentrations of boron 10 shielding: 5% and 30%. The detector was shielded on the two sides facing the nearest wall, top, bottom, and part of the leftmost side (see Figure 2). The side facing the beamline was left open in order to minimize attenuation of neutron energies as they approach MicroCHANDLER. In addition to this open face, openings on the left and right sides allow airflow through the detector to cool the electronics. MicroCHANDLER was placed directly in front of the beam 3.315m away from the end of the beamline and oriented such that the beam was pointed at the center of one of the faces of the black container. This was to ensure that the neutron flux was more-or-less evenly distributed in the vertical plane facing the beam.

### 2.2. The Beam

For the data runs analyzed in this study, the tandem particle accelerator generated a steady beam of deuterons ( $d$ ) to be fired onto a tritium target with a frequency of 78kHz. Near the end of the beamline tritium interacts with the deuterons ( $d, n$ ) to create bursts of deuterium-tritium ( $dt$ ) neutrons that continue in the direction of the incident deuterons. Due to the extensive use of this accelerator beamline over numerous decades, much deuterium has become embedded in the beamline and target, creating a source of deuterium-deuterium ( $dd$ ) neutrons in addition to the  $dt$  neutrons. Both the  $dt$  and  $dd$  neutron peaks appear in the data, but will not be directly relevant to this study. Additionally, the deuterons have to go through a titanium window to get to the tritium target. When the deuterons go through this window, they generate gamma rays, a byproduct of beam production. These gammas arrive in the detector about 11ns after the deuterons hit the tritium target and are very easy to identify in the delta time plots. This property makes them easy to remove later in the data analysis process.

Further, the deuteron beam passes through a beam pulse monitor (BPM) which is used to determine the timing of beam on

target. The BPM consists of a coil of copper wire wrapped around the beamline just before the deuterons hit the target material. Because the deuterons are charged, they induce an electric pulse in the BPM coil which creates a signal that can be used to track the frequency of the particles and the stability of the beam.



Figure 2. MicroCHANDLER placed within an enclosure of borated polyethylene. The pink sheets contain a 5% concentration of Boron 10 while the black sheets contain 30%.

### 2.3. Data Acquisition Procedure

During the data acquisition process, we utilized an event window with a length of  $2\mu\text{s}$  with a sample size of 129 ticks. To reduce the number of background events that coincide with the BPM, we internally triggered on events in the detector exceeding 45 ADC above the baseline. To determine what events were actually caused by the neutron beam and not the environmental background, the BPM was recorded on a channel in the trigger window. This allows us to find events that contain the BPM so that we can filter the data to determine which data are actually beam-correlated and filter it accordingly.

Lastly, two different types of calibration runs were taken while at TUNL. Firstly vertical muon runs were taken during the night while the beam was off. Secondly, a sodium 22 source was placed at different locations around the detector and several ten minute runs were taken so that we would have those calibration points in addition to the vertical muon peaks.

## 3. Data Analysis

### 3.1. ADC Plots

Numerous data acquisition runs were taken while at TUNL, but only four of those were used for the following ADC and  $\Delta t$  analysis (runs 1021, 1022, 1028, and 1031). These four runs were all taken under the same beam energy and rep rate. The important difference between these runs is the amount of time the BPM pulse was delayed by a delay generator. The beam rep rate for these runs was about 78kHz which indicates a beam period of  $12.8\mu\text{s}$  and since the event windows were only  $2\mu\text{s}$  long, varying the delay times allowed us to place the event window at different places within those  $12.8\mu\text{s}$  between beam pulses. Note

that for this study, all delays are described in terms of their time relative to the first BPM pulse in a given beam window. So, our  $25\mu\text{s}$  delay is effectively  $-0.6\mu\text{s}$  since one beam window is  $12.8\mu\text{s}$  (and two bpm windows are  $25.6\mu\text{s}$ ).

In the ADC plots for these runs, one notices that there is a distinct shoulder-like peak that appears when we include the events that contain the BPM pulse, indicating that the event is beam-correlated (see above for definition and see Figure 3). This feature typically ranges from about 300 ADC to 500 ADC. To get a sense of what the background is like at TUNL, we took a ten minute data acquisition run when the beam was off using the same internal trigger. The data from this run is used as a model for the background in Figure 3. Note that both runs 1031 and 1029 have been scaled so that they contain a comparable number of entries in each ADC plot. Both runs were divided by their respective run times so that both were plotted with an "effective" one minute duration. Moreover, the background run had to be scaled by  $2/12.8$  (event window duration time / time between beam pulses) in order to compensate for the fact that the background run did not have a BPM. Without a BPM, the background run would essentially contain any event that surpasses the ADC threshold; therefore, we need to scale this run by the ratio of time for the event window by the amount of time between beam pulses to obtain a better estimate for the background we would see within the event window. Note that there are still problems with the background approximation that have yet to be worked out.

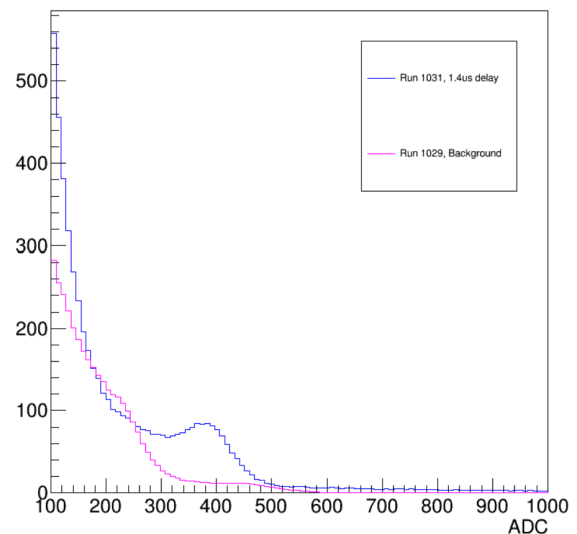


Figure 3. ADC plot for events containing the BPM during run 1031 with an effective delay of about  $1.4\mu\text{s}$ . Note that this plot is the summation of the histograms from each PMT channel.

### 3.2. Delta Time ( $\Delta t$ ) Plots

Having confirmed that the feature from the ADC plots is actually beam-correlated and not an artifact of the background, the

events from the detector were plotted over time by creating  $\Delta t$  plots. In these plots, both the highest peak in the event window and the BPM pulse were given a timestamp. The difference between these two values was calculated and dumped into a histogram. Since each of these  $\Delta t$  histograms is only about  $2 \mu s$  in time multiple runs were stitched together to span a greater period in time (see Figure 4).

The process of stitching histograms together is rather straightforward. First, each individual run's  $\Delta t$  histogram was offset by its delay time relative to the  $2 \mu s$ . Once the runs were properly offset, each was dumped into a combined histogram. From this point, there were regions where more than one  $\Delta t$  plots overlapped. In these regions the histogram was scaled by either  $1/2$  or  $1/3$  depending on whether two or three histograms overlapped. From there, we fit a curve of the form  $f(t) = e^{(p_0 + p_1 * t)} + p_2$  where  $p_i$  ( $i \in 0, 1, 2$ ) is a constant parameter. Lastly, the region containing the gamma peak had to be omitted from the fit in order to prevent it from skewing the curve. To do so, the error was suppressed to zero. This worked since ROOT's fit operator will only fit a function over bins that have a non-zero error.

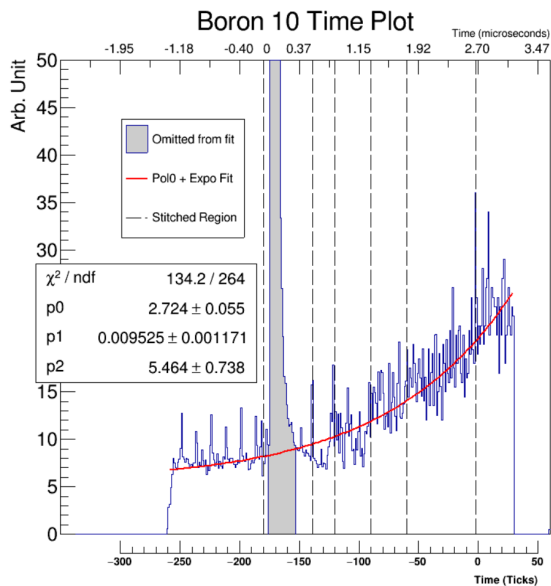


Figure 4. Stitched histogram for runs 1021, 1022, 1028, and 1031. The gray region is the gamma peak and was omitted from the fit entirely.

Also, note that this time plot is about  $4.4 \mu s$  in duration.

Figure 4 is divided into seven differently scaled regions using six dashed lines. From left to right the scaling factors are as follows:  $1, \frac{1}{2}, 1, \frac{1}{2}, \frac{1}{3}, \frac{1}{2}, 1$ . These scaling factors allowed us to accommodate the overlap between histograms. Looking at the fit function in Figure 4, a growth structure is evident given the  $p_1$  value of  $(9.525 \pm 1.171) \times 10^{-3}$  in  $1/\text{ticks}$  or  $(0.6143 \pm 0.0755) \mu s^{-1}$ . However, while Figure 4 was fit with an exponential curve, it is unclear whether that is the proper fit for this time structure. A better model is required to determine the true form of the fit function will take.

#### 4. What is This Turn-On?

Initially, our hypothesis was that the bump in the ADC histogram corresponds to gammas being emitted from some neutron capture process on boron 10 in the BP shielding placed around the detector. This would be a very convenient solution to our question since it should match the growth structure well enough. However, calibrating the ADC scale on our energy histograms suggests that the peak we see has too low of an ADC value to be a result of a 4.4 MeV gamma emitted from neutron captures on boron 10. To be sure of this, a calibration run was performed while at TUNL using a  $^{22}\text{Na}$  source placed on top of the detector.

To obtain a calibration point from these events, we needed  $^{22}\text{Na}$  ADC plots with a decent resolution. Examining what the ADC plots look like in each cube of a given layer within the detector is a great way to achieve higher resolution. In order to isolate one specific cube, we selected events wherein the maximum pulse heights in the x and y axes correspond to the channels that intersect that cube. For example, for the cube that intersects PMT channels 2 and 11, we selected events where the highest pulse in the x axis was in channel 2 and that of the y axis was in channel 11. These cube-specific events were recorded in both the x and y axis PMT for a given horizontal plane of cubes in the detector. This process was performed for the top layer of the detector for the  $^{22}\text{Na}$  run and several other "beam-on" runs in order to compare the two types of runs at a higher resolution (see Figures 5 and 6).

From Figure 5, two different types of attenuation are evident. The first is neutron attenuation and it pertains to the number of neutrons that reach the different PMTs of the detector. Neutron attenuation is simply an effect brought on by the fact that as neutrons penetrate deeper into the detector, they are more likely to have already scattered off of atoms inside the plastics and deposited some of their energy into the detector. This property decreases the number of neutrons that reach the PMTs further back in MicroCHANDLER. In Figure 5, the beam moves from right to left. Notice that neutron attenuation is the reason that the statistics are slightly poorer for the leftmost column than for the rightmost.

The second type of attenuation is an effect of photons Compton scattering off of molecules within the plastics. Photons generated in the cubes furthest away from the PMTs in a given layer will have more opportunities to Compton scatter as they move towards a PMT. This effect manifests in Figure 5 by shifting the peaks to lower ADC counts. Note that in the top row of plots, the peak sits on a lower ADC value than those of the lower row. These differences are due to the photon attenuation.

This  $^{22}\text{Na}$  run gives us a calibration point of 1060keV at about  $230 \pm 5$  ADC since  $^{22}\text{Na}$  produces 1.274 MeV gammas. Assuming a relatively linear energy response of the detector around 230 ADC, we would expect the peak (with an ADC value of about  $450 \pm 30$  ADC) to correspond to an energy value around  $2074 \pm 140$  keV. This energy value corresponds to the

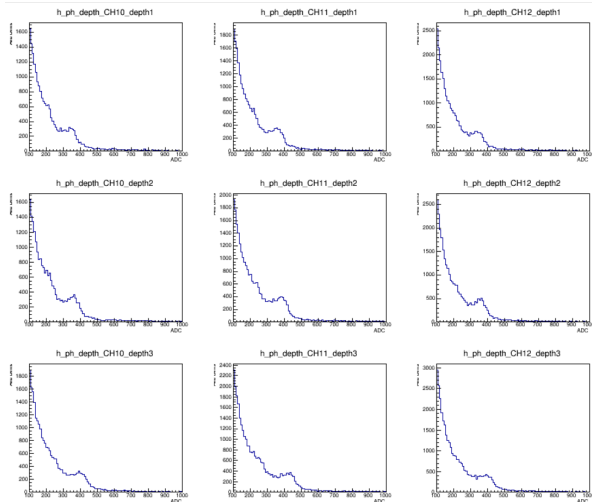


Figure 5. ADC plot for the top 3x3 layer of cubes in the detector as registered by the three PMTs on the y-axis. These plots are a summation of seven different runs where bpm=on was required.

energy of gammas emitted by neutron captures on hydrogen which can Compton Scatter a maximum energy of about 1940keV.

Hydrogen captures are a viable candidate for explaining the features displayed in the energy plots and time plot since the energy of the peak corresponds to a gamma given off by neutron captures on hydrogen. Although the cross-section for thermal neutrons on hydrogen (on the order of one barn) compared to that of boron 10 (on the order of 1000 barns), the abundance of hydrogen in BP compared to boron 10 should compensate for the significantly smaller cross-section, especially in the BP sheets with only 5% boron concentration.

## 5. Conclusion and Next Steps

Looking at Figure 4, it is pretty clear to see that even for run 1028 (which occupies the left-most end of the time plot), there is still an indication of some sort of activity in the detector just before BPM pulse. It is unclear at this moment how much of this activity is from the flat background and how much is from remaining thermal neutrons capturing in the BP from the previous beam pulse. Yet, even without knowing whether this activity is background radiation or neutron capture gammas, we can still conclude that a  $25\mu s$  delay provides less capture gammas than the other delay times.

Not only did this study provide evidence that a  $25\mu s$  delay provides minimal capture gammas, this study has also provided evidence that the BP provides a 2.2 MeV gamma which manifests itself in MicroCHANDLER. This reliable gamma peak can be used as a calibration point for future runs.

As mentioned before, the data taken for this study was primarily preliminary so that we can go back to TUNL later this year to obtain more data to do a full analysis of MicroCHANDLER's response to fast neutrons. Having said that, there are

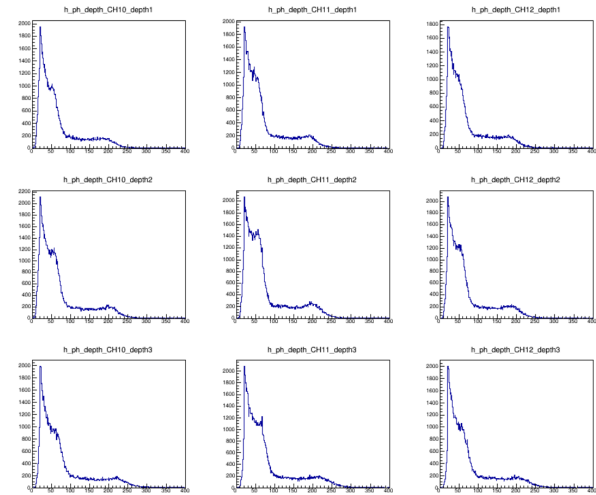


Figure 6. Top layer of cubes in the detector for the ten minute  $^{22}\text{Na}$  calibration run as registered by the three PMTs on the y-axis. Note that the  $^{22}\text{Na}$  source was placed directly above the center cube in this plot.

some essential next steps that ought to be taken during the next data acquisition period this year and the analysis therein.

Firstly, to confirm that what we see in Figure 4 is actually a neutron capture turn-on, we need to find the turn-over point in the time structure that corresponds to the moment when the majority of neutron captures have already occurred in a given beam period. Additionally, we would need to find evidence of some sort of decay structure after the turnover point. For the moment, our data from Figure 4 suggests that, for constant beam conditions, we are only seeing a mere  $4.4\mu s$  out of a  $12.8\mu s$  beam period window. More data acquisition runs should be taken using a beam energy of 19MeV and a frequency of 78kHz to recreate the conditions used in this study. From there, utilize a delay generator to delay the BPM (starting at  $0\mu s$ ) and taking 30 minute runs at  $2\mu s$  or  $1.5\mu s$  delay intervals until reaching a final delay time of  $14-16\mu s$ . These data points will provide adequate coverage over the beam period window to determine whether there actually is both an exponential-like growth and decay in time. This would corroborate the claim that the energy peak that we see is actually caused by neutron captures on hydrogen within the borated polyethylene. It may also be beneficial to try a lower beam rep rate (if possible). This would lengthen our beam period to see if the neutron captures disappear from the event window altogether.

Determining the linearity of energy response within the detector should also be a goal moving forward. One way of doing this would be to utilize another gamma source in addition to the  $^{22}\text{Na}$  source. Perhaps a  $^{60}\text{Co}$  or a  $^{133}\text{Ba}$  source would be useful to obtain more calibration points. From there, we can plot the response ADC counts as a function of energy in keV to see if there is a linear slope. If the linearity is strong for regions that we are looking at, we can fit the plot with a line, and the slope of that line to get a conversion constant between ADC and energy.

Lastly, a model should be developed in the future so that one

can better fit a curve to the turn-on time structure and therein perform a stronger analysis. With these changes we have suggested, the next round of analysis should run smoothly after we take better data at TUNL again in September.

## 6. Acknowledgments

We want to thank Phil Barbeau and the staff at TUNL for operating the tandem particle accelerator and beamline along with Camillo Mariani for advising the undergraduate students in the Virginia Tech REU program. Work performed by Jacob Steenis could be made possible by a grant from the National Science Foundation and its Research Experiences for Undergraduates program.

## References

- A. Haghghat et al, 2018. Observation of Reactor Antineutrinos with a Rapidly-Deployable Surface-Level Detector, Blacksburg, Virginia, United States.
- C. Grieb, J. M. Link, and R. S. Raghavan Probing active to sterile neutrino oscillations in the LENS detector, Blacksburg, Virginia, United States.
- Y. Abreu et al. A novel segmented-scintillator antineutrino detector, (SoLid Collaboration) .